Moschonas, I. F. & Kappos, A. J. (2011). Generalized fragility curves for bearing-supported skew bridges, for arbitrary angle of incidence of the seismic action. In: M. Papadrakakis, M. Fragiadakis & V. Plevris (Eds.), Computational Methods in Structural Dynamics and Earthquake Engineering. (pp. 3486-3508). Athens: Institute of Structural Analysis and Antiseismic Research. ISBN 978-960-99994-1-0

COMPDYN 2011
III ECCOMAS Thematic Conference on
Computational Methods in Structural Dynamics and Earthquake Engineering
M. Papadrakakis, M. Fragiadakis, V. Plevris (eds.)
Corfu, Greece, 26–28 May 2011

GENERALIZED FRAGILITY CURVES FOR BEARING-SUPPORTED SKEW BRIDGES, FOR ARBITRARY ANGLE OF INCIDENCE OF THE SEISMIC ACTION

Ioannis F. Moschonas[1], **Andreas J. Kappos**[1]

[1] Department of Civil Engineering
Aristotle University of Thessaloniki, Greece
imoschon@civil.auth.gr; ajkap@civil.auth.gr

Keywords: Bridges, Vulnerability assessment, Fragility curves, Pushover analysis, Damage states, Angle of Incidence.

Abstract. *In a previous work by the authors and their co-workers an analytical methodology for the derivation of seismic fragility curves for bridges was proposed. Bridges were classified into three main categories according to their seismic energy dissipation mechanism: bridges with yielding piers of the column type, bridges with bearings and non-yielding piers of the wall type, and bridges with bearings and yielding piers of the column type. Then, damage states were defined using deck displacement at characteristic points of 'typical' bridge pushover curves, which are related to the seismic energy dissipation mechanism, consistently with the proposed classification scheme. Only one horizontal component of the seismic action was considered to act along the principal directions of the bridge. This methodology was subsequently extended by the authors to take into account the angle of incidence of the seismic action, considering only the single-component case. In the present work the methodology is further extended to the general case wherein the minor principal horizontal component of the earthquake is also taken into account (dual-component seismic action). Furthermore, damage states for bridges with bearings are redefined in a broader manner, to take into account biaxial shear effects, and all possible failure mechanisms of the bearings. The methodology is applied here to a skew bridge, subjected to either single- or dual-component seismic action. The main difference between straight and skew bridges is that the modal principal bridge directions are rotated with respect to the geometric principal bridge directions, for a specific angle of incidence. The proposed methodology is formulated in terms of modal principal directions. The CQC rule is used for the combination of the projections of the control point displacement and of the base shear in the single-component case, while in the dual-component case the SRSS rule is used and it is found adequate for all excitation angles. From the derived generalized fragility curves it is concluded that when the minor principal horizontal component of the earthquake is taken into account, bridge fragility is significantly increased, while it remains practically unaffected by the angle of incidence.*

1 INTRODUCTION

Various analytical methodologies proposed in the past for the vulnerability/fragility assessment of bridges in Europe [8], the US [6, 9, 10, 13], and Japan [4], address only one horizontal component of the seismic action (single-component seismic action) acting along the longitudinal or transverse direction of the bridge. Hence, an issue that has to be addressed is the assessment of bridge vulnerability/fragility in the general case where the seismic excitation acts at an arbitrary angle. The first attempt in this direction was made by Shinozuka et al. [12] who proposed an analytical methodology based on dynamic inelastic analysis for single-component seismic action. Damage states were defined only for bridges with inelastic piers, in terms of displacement ductility of pier critical sections.

Recently the authors have developed a methodology for the derivation of fragility curves for arbitrary angle of incidence of the seismic action [7] extending their previously proposed methodology [8], which is based on static nonlinear (pushover) analysis. At first, static nonlinear analysis was extended to take into account the angle of incidence of the seismic action; it is noted that on this topic only two previous attempts have been made in [14] and [15], both of them focusing on the estimation of the critical angle of incidence of the seismic action, rather than on the derivation of pushover curves. Two methodologies were proposed for deriving pushover curves for arbitrary angle of incidence of the single-component seismic action. According to the first one, an effective mode shape is determined in the direction of the seismic action, while according to the second one the response along the principal bridge directions is combined in order to derive the response in the direction of the earthquake. The two methods were both applied to a symmetric overpass bridge and the results were evaluated against those from nonlinear response-history analysis (NLRHA). It was concluded that the first method is valid only in the period range where the equal displacement approximation is valid, while the second one is valid for all periods. Besides the extension of static nonlinear analysis, damage state definitions were also extended to take into account the effect of the angle of incidence of the seismic action.

In the work presented herein, the methodology for the derivation of static pushover curves and fragility curves for arbitrary angle of incidence of the seismic action is extended to account for dual-component seismic action. Static nonlinear analysis for arbitrary angle of incidence is carried out using the second of the previously proposed methods [7], due to its broader range of application; the method is further extended to account for biaxial bending effects in critical pier sections and for biaxial shear effects in the bearings. Regarding damage state definitions, in particular for bearing-supported bridges, damage states are defined taking into account the biaxial deformation of the bearings. Furthermore, the last damage state is defined on the basis of the ultimate shear deformation, as it is derived considering all possible failure mechanisms of the bearings. Finally, the proposed methodology is applied to a skew bearing-supported bridge and conclusions are drawn regarding the effect of dual-component action and of angle of incidence.

2 METHODOLOGY FOR THE DERIVATION OF FRAGILITY CURVES

2.1 Modelling of the seismic action

The earthquake ground motion is analyzed into three principal components E_I, E_{II} and E_{III} linearly independent (or statistically linearly uncorrelated) directed along a set of principal axes *O-I-II-III*. Components E_I and E_{II} are the horizontal ones, with the first one having the maximum intensity (E_I = major horizontal component, E_{II} = minor or secondary horizontal component).

The simpler approach is to consider only the major horizontal earthquake component (single-component seismic action) acting at an angle *a* with respect to the bridge longitudinal axis (Fig. 1). Thus, the axis system *O-I-II-III* is considered identical with system $O\xi\eta\zeta$ which is rotated by an angle *a* with respect to the bridge axes *Oxyz*. Thus, the major earthquake component E_I acts along $O\xi$ axis and for this reason it will be referred to as E_ξ.

The proposed methodology for deriving pushover curves for arbitrary angle of incidence of the seismic action described in the following paragraphs is based on the combination of longitudinal and transverse responses. Therefore, it is more convenient to analyse the major earthquake component into two components $E_x=E_\xi \cdot \cos a$ and $E_y=E_\eta \cdot \sin a$ (Fig. 1) acting along the longitudinal and transverse direction, respectively. Components E_x and E_y have identical time-histories (accelerograms), thus they are linearly dependent or statistically linearly fully correlated.

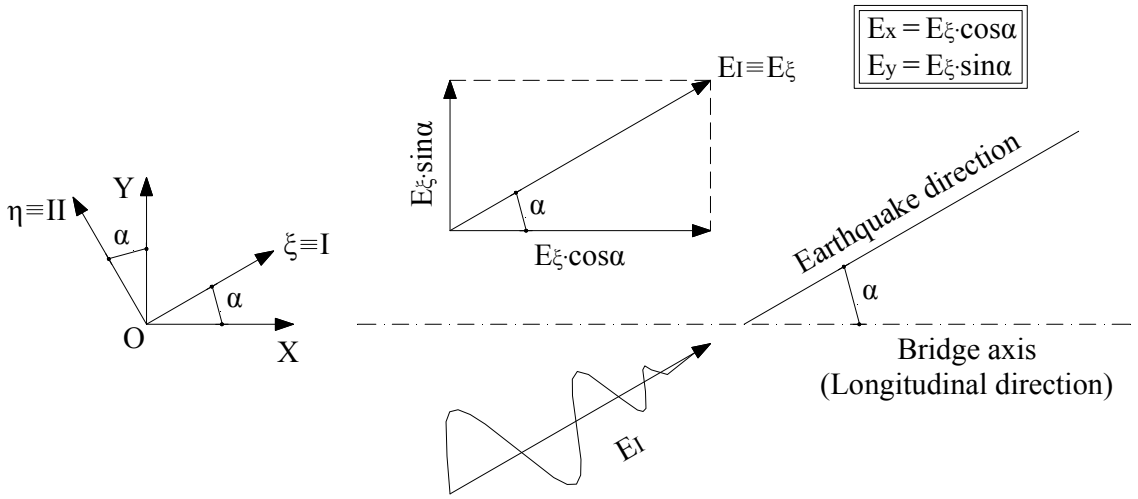

Figure 1: Single-component seismic action acting at an arbitrary angle of incidence.

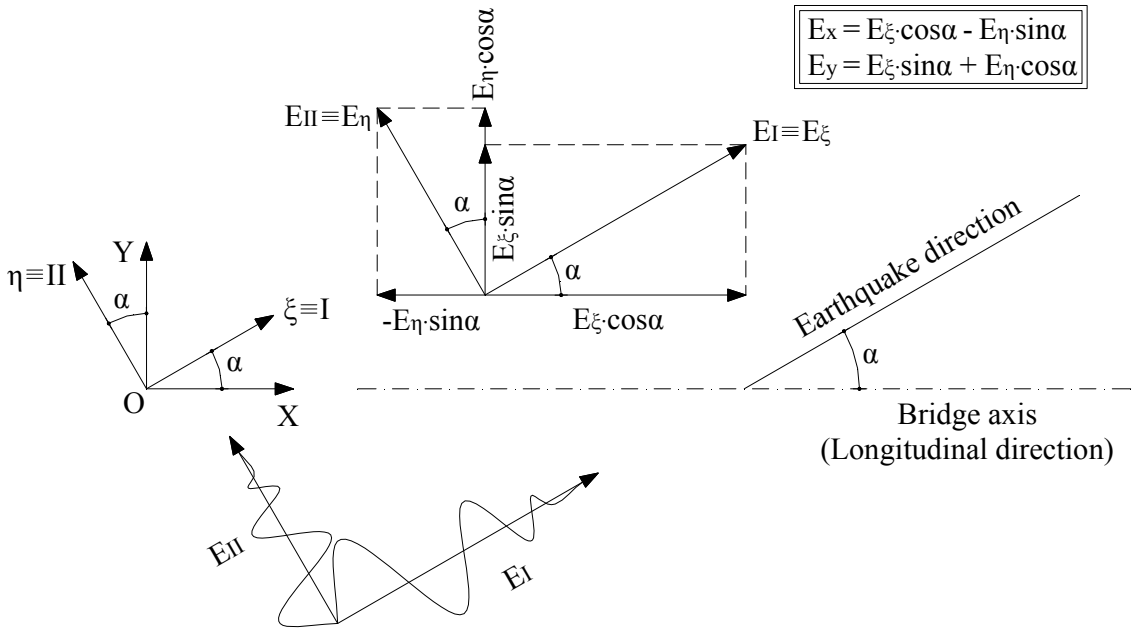

Figure 2: Dual-component seismic action acting at an arbitrary angle of incidence.

In the general case the minor horizontal earthquake component, $E_{II} \equiv E_{\eta}$, is also considered (dual-component seismic action) (Fig. 2) and it is normal to the major horizontal component E_I, which acts at angle a with respect to the longitudinal bridge axis X (i.e. the minor component acts at an angle α with respect to the Y-axis). The components acting along the longitudinal and the transverse bridge directions are $E_x = E_{\xi} \cdot \cos\alpha - E_{\eta} \cdot \sin\alpha$ and $E_y = E_{\xi} \cdot \sin\alpha + E_{\eta} \cdot \cos\alpha$. These components are a linear combination of E_{ξ} and E_{η}, thus they are linearly dependent or statistically linearly correlated. For excitation angles 0°, 90°, 180° and 270° components E_x and E_y become identical with the principal horizontal components $E_I \equiv E_{\xi}$ and $E_{II} \equiv E_{\eta}$, thus they have quite different time-histories, i.e. they are linearly independent or statistically linearly uncorrelated.

Only natural earthquake records can be analyzed into principal components. Hence, in the case where a code-type response spectrum, or spectrum-compatible artificial accelerograms are utilized, a proper value for their intensity ratio is required; based on the available literature [5] a value of 0.70 can be reasonably adopted.

2.2 Derivation of pushover curves

Having modelled the seismic action appropriately, i.e. analyzing it into the components acting along the longitudinal and transverse directions, the next step for the derivation of pushover curves for arbitrary angle of incidence of the seismic action is to take into account the interaction between biaxial bending moments and axial force (PMM interaction) at critical pier sections and/or the interaction between biaxial shear forces and axial force (PFF interaction) in the bearings.

In the first step of the method, the bridge is analyzed for a low earthquake intensity level (e.g. 0.1g) for which the response along both principal bridge directions remains within the elastic range. Then, the displacements of the selected control point along the longitudinal and transverse bridge directions, $u_{L,el}$ and $u_{T,el}$, are calculated using elastic response spectra, and from them the corresponding rotations ($\theta_{x,el}$ and $\theta_{z,el}$) and moments ($M_{x,el}$ and $M_{z,el}$) of the critical pier sections, as well as the corresponding shear deformations ($\gamma_{x,el}$ and $\gamma_{z,el}$) and forces ($F_{x,el}$ and $F_{z,el}$) in the bearings along their principal axes, are estimated. The moment ratio $M_{x,el}/M_{z,el}$ (Fig. 3) and the bearing shear force ratio $F_{x,el}/F_{z,el}$ remains constant also for higher earthquake intensity levels so long as the loading is monotonically increasing and the response along both principal bridge directions remains elastic. For a certain earthquake intensity level the pier critical section, or an individual bearing, yields under a moment M^{y}_{int} (Fig. 3) or force F^{y}_{int}, respectively (the subscript *int* indicates that the point lies on the interaction curve). This means that the critical section or the bearing yields under biaxial conditions earlier than in the case where the moment vector is normal, or the force vector is parallel, to one of the principal directions. Then, the (idealised as bilinear) M-θ or F-γ diagrams along the principal directions of critical pier sections or bearings are modified using the reduced values of yield moments or yield forces, respectively.

Finally, the selection of an appropriate axis to project the displacement of the control point and the base shear force of the bridge along the longitudinal and the transverse direction is needed, so that the pushover curve can be plotted. An obvious choice is the axis $O\xi$ of the major earthquake component $E_I \equiv E_{\xi}$. From the two approaches proposed in [7] the one based on the combination of responses along the bridge's principal directions is used here, for the reasons explained earlier in the paper. The successive steps of the methodology proposed for deriving the pushover curve are the following:

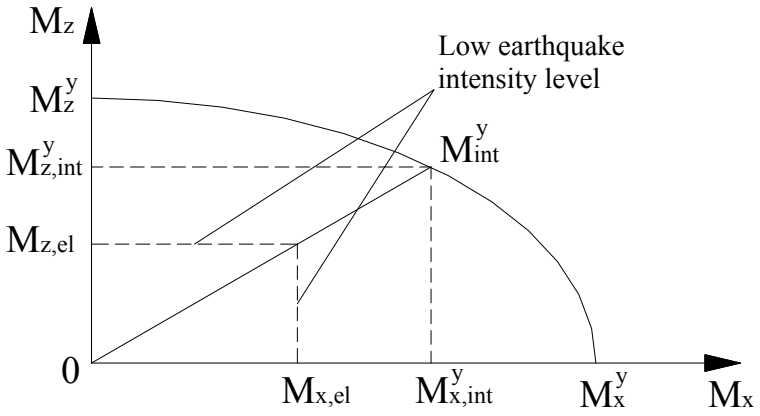

Figure 3: Elliptically idealised moment interaction diagram of a critical R/C pier section.

Step 1: For a given dual-component seismic action E (code-type spectra or natural records) whose major component acts at an angle a, the corresponding component response spectra E_x and E_y (Fig. 2) are calculated and are scaled to increasing levels of earthquake intensity (0.1g, 0.2g,…, $A_{g,u}$·g) until the bridge reaches its ultimate point (bridge failure) at the intensity level $A_{g,u}$.

Step 2: For a low earthquake intensity level (e.g. 0.1g), for which bridge response along both its principal directions remains elastic, the moments $M_{x,el}$ and $M_{z,el}$ of critical pier sections and the shear forces $F_{x,el}$ and $F_{z,el}$ of bearings along their principal directions are calculated. The resulting moment ratios $M_{x,el}/M_{z,el}$ and shear force ratios $F_{x,el}/F_{z,el}$ are subsequently used in the corresponding interaction diagrams (Fig. 3) to reduce yield moments of critical pier sections and/or yield shear forces of bearings; the reduced values are introduced in the M-θ or F-γ diagrams for the principal directions of critical pier sections and of individual bearings.

Step 3: A 'standard' pushover analysis is performed separately along the longitudinal (0°) and the transverse direction (90°), for lateral force patterns compatible with the corresponding prevailing mode. Then, the derived pushover curves are idealised as bilinear ones [11] and they are converted to spectral pushover curves ('capacity curves' [3]) of the inelastic equivalent SDOF corresponding to the prevailing mode of each principal bridge direction.

Step 4: At each earthquake intensity level the displacement $u_{L,max}$ along the longitudinal direction and $u_{T,max}$ along the transverse direction are calculated using inelastic spectra. Then, the corresponding base shears V_{bL} and V_{bT} are extracted from the database of each individual pushover analysis and the projections of these two quantities on the axis of earthquake action (Fig. 2) are taken, i.e.

$$u_{L,proj} = u_{L,\max} \cdot \cos\alpha, \;\; V_{bL,proj} = V_{bL} \cdot \cos\alpha \tag{1}$$

$$u_{L,proj} = u_{T,\max} \cdot \sin\alpha, \;\; V_{bT,proj} = V_{bT} \cdot \sin\alpha \tag{2}$$

Then, the projections are combined using the SRSS rule, the CQC rule or the ABS rule, since these response quantities are not simultaneous, for the calculation of the displacement u_ξ and the base shear force $V_{b\xi}$ in the earthquake direction. In case of the SRSS rule, u_ξ and $V_{b\xi}$ are calculated using the following relationships:

$$u_\xi = \sqrt{u_{L,proj}^2 + u_{T,proj}^2} = \sqrt{u_{L,\max}^2 \cdot \cos^2\alpha + u_{T,\max}^2 \cdot \sin^2\alpha} \tag{3}$$

$$V_{b\xi} = \sqrt{V_{bL,proj}^2 + V_{bT,proj}^2} = \sqrt{V_{bL}^2 \cdot \cos^2\alpha + V_{bT}^2 \cdot \sin^2\alpha} \quad (4)$$

Step 5: Step 4 is repeated for all earthquake intensity levels (0.1g, 0.2g,…, A_{gu}·g) until the bridge reaches its ultimate point in either principal direction. The pushover curve referring to the earthquake direction is plotted using u_ξ–$V_{b\xi}$ points.

2.3 Definition of damage states

The first step for defining damage states is their qualitative (descriptive) definition. Here the corresponding definitions of HAZUS [3] are adopted which are based on bridge damage data from the Loma Prieta and Northridge earthquakes [1]. Thus, four damage states, in addition to the No-Damage state (DS0), are defined: Minor/Slight Damage (DS1), Moderate Damage (DS2), Major/Extensive (DS3) Damage, and Failure/Collapse (DS4).

Then, damage state descriptive definitions are quantified in terms of bridge deck displacement δ_ξ (global damage parameter) along the earthquake direction. Apart from bridge damage, i.e. damage developed due to plastic hinge formation in the piers and/or yielding of bearings, damage developed at the abutment-backfill system due to its activation after the longitudinal gap closure is also taken into account. Damage states due to bridge damage are defined using bridge deck displacement δ_ξ at characteristic points of 'typical' bridge pushover curves for a given earthquake direction a, which are defined on the basis of the seismic energy dissipation mechanism consistently with the classification scheme proposed in [8]. Damage states due to damage developed at the abutment-backfill system are also defined using bridge deck displacement, and complement the corresponding damage state definitions referring to bridge damage. The final threshold value of displacement for each damage state is taken as the minimum of the two threshold values for damage to the bridge (piers, bearings) and damage to the abutment-backfill system.

2.3.1 Bridges with yielding piers of the column type

In bridges with inelastic piers of the column type the 'typical' pushover curve for seismic action acting at an angle a along the axis $O\xi$ is shown in Fig. 4. The first branch of the pushover curve corresponds to all the seismic intensity levels for which the response in both bridge directions remains in the elastic range, and terminates at the first plastic hinge formation (Point A). The second branch of the pushover curve corresponds to the successive plastic hinge formation (development of plastic mechanism) and terminates at the intensity level for which the last plastic hinge forms (Point B). The third branch of the pushover curve terminates at the first failure of a pier (Point C). Subsequent to this point progressive failure of the bridge occurs, with successive pier failures, as shown in Fig. 4.

Idealizing the pushover bridge curve as bilinear, the second branch corresponding to the plastic hinge formation stage (branch AB) is reduced to a single point (named conventional yield point) and the branch after Point C corresponding to the failure mechanism is reduced to another single point (named bridge ultimate point) using a strength drop criterion for the bilinearization and the assumption of equal areas between the initial and the idealised pushover curves [11]. The four damage states are then defined on the bilinearised bridge pushover curve as described in Table 1. The first damage state (DS1: Minor Damage) is defined at the elastic branch (at 70% of conventional yield displacement, since, as described previously, actual yielding occurs before the conventional yield point), while the last damage state (DS4: Failure/Collapse) is defined at the ultimate bridge point, defined as previously. The two intermediate damage states (DS2: Moderate Damage and DS3: Major/Extensive Damage) are defined differently for high ductility bridges ($\mu_u \geq 3.0$) and for low-to-moderate

ductility bridges (μ_u<3.0). More specifically, in high ductility bridges intermediate damage states are defined at bridge displacements corresponding to ductility levels 1.5 and 3.0, while in low-to-moderate ductility bridges are defined at displacements equally spaced (1/3 and 2/3) along the post-yield branch.

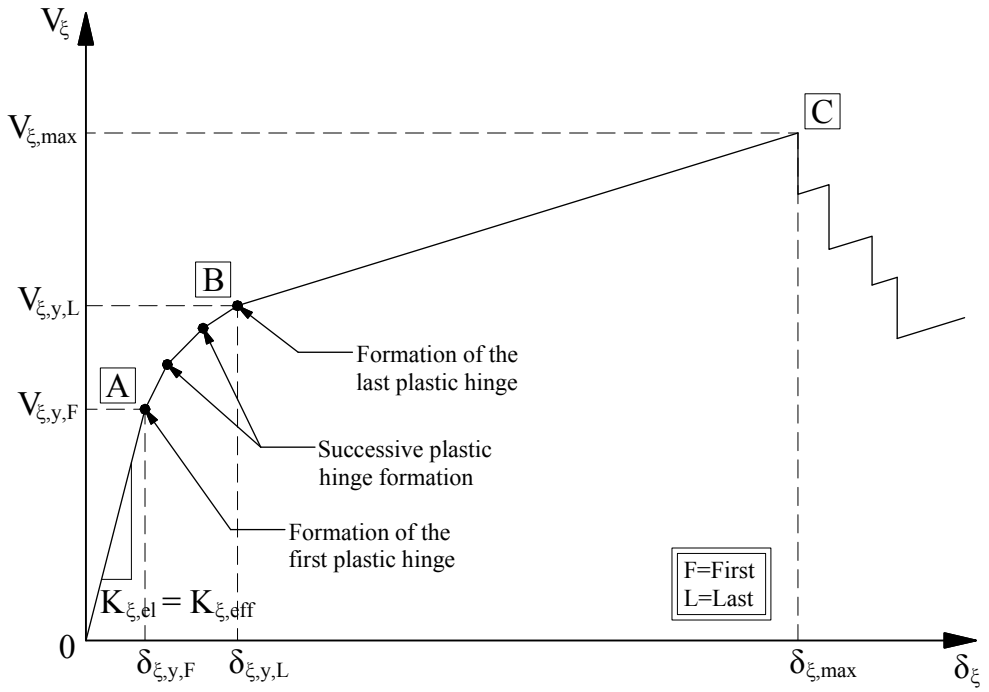

Figure 4: 'Typical' pushover curve of bridges with yielding piers of the column type.

a/a	Damage State	Threshold values of δ_ξ	
		$\mu \geq 3.0$	$\mu < 3.0$
DS1	Minor/Slight	$> 0.7 \cdot \delta_{\xi,y}$	$> 0.7 \cdot \delta_{\xi,y}$
DS2	Moderate	$> 1.5 \cdot \delta_{\xi,y}$	$> \delta_{\xi,y} + (1/3) \cdot (\delta_{\xi,u} - \delta_{\xi,y})$
DS3	Major/Extensive	$> 3.0 \cdot \delta_{\xi,y}$	$> \delta_{\xi,y} + (2/3) \cdot (\delta_{\xi,u} - \delta_{\xi,y})$
DS4	Failure/Collapse	$> \delta_{\xi,u}$	$> \delta_{\xi,u}$

Table 1: Damage state definitions for bridges with yielding piers of the column type.

2.3.2 Bridges with bearings and non-yielding piers of the wall type

In this type of bridge the shape of the 'typical' pushover curve is similar to that of the previous type, replacing yielding and failure of critical pier sections with yielding and failure of bearings (or groups of bearings in the common case where more than one bearings are placed at the top of a pier) (Fig. 5-solid line). Whenever seismic links (stoppers) are present at the top of the piers an apparent hardening-softening is noticed due to their successive activation and failure, respectively (Fig. 5-dotted line, see discussion in [8]).

Damage states for this bridge type are defined as follows: Firstly, damage states for a single bearing are defined (Table 2) using shear deformation, γ_{bi}, as damage parameter. Then, the deformation of the equivalent single bearing, γ_{eq}, is calculated as the average of the deformations of all bridge bearings, i.e.

$$\gamma_{eq} = \frac{\sum_{i=1}^{N} \gamma_{bi}}{N} \tag{5}$$

where: γ_{bi} = shear deformation of single bearing *i*
γ_{eq} = shear deformation of the equivalent single bearing and
N = total number of bridge bearings

hence damage state definitions for the single bearing (Table 2) can be used also for the entire bridge. Alternatively, the corresponding bridge displacement δ_ξ (Table 2) can be used for damage state definitions. More specifically, the first damage state is defined using the yield shear deformation γ^y_{int}, which lies on the interaction curve and is derived for low earthquake intensity level. The other three damage states are defined reducing the threshold values for the uniaxial shear deformation of bearings (1.5, 2.0 and γ_u) using the minimum of the ratios $\gamma^y_{x,int}/\gamma^y_x$ and $\gamma^y_{z,int} / \gamma^y_z$ (Table 2).

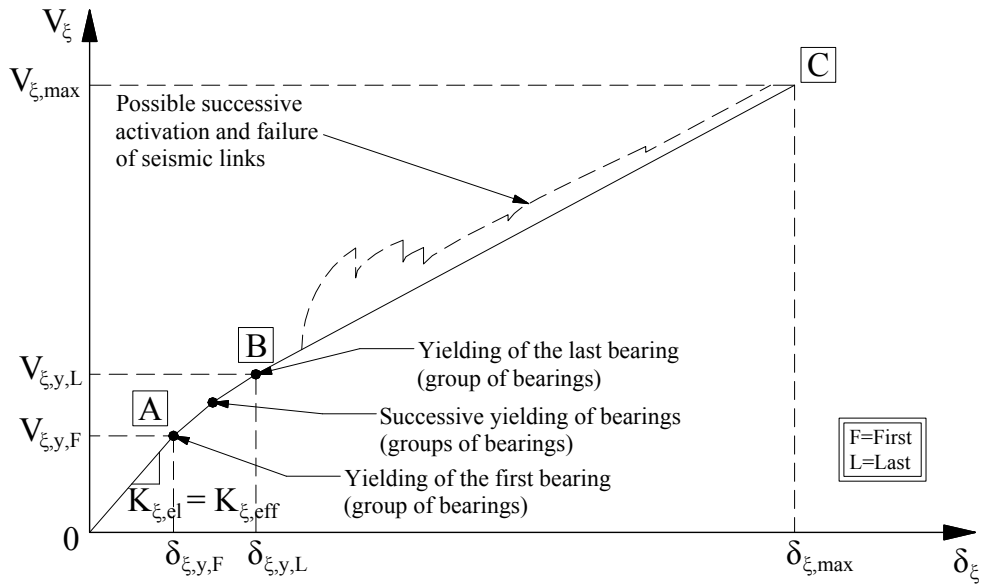

Figure 5: 'Typical' pushover curve of bridges with bearings and non-yielding piers of the wall type.

a/a	Damage State	Threshold values of γ_{bi}, γ_{eq}	δ_ξ
DS1	Minor/ Slight	$> \gamma^y_{\text{int}}$	$> \delta_\xi(\gamma_{eq,DS1})$
DS2	Moderate	$> 1.5 \cdot \min\left[\gamma^y_{x,\text{int}} / \gamma^y_x, \gamma^y_{z,\text{int}} / \gamma^y_z\right]$	$> \delta_\xi\left(\gamma_{eq,DS2}\right)$
DS3	Major/ Extensive	$> 2.0 \cdot \min\left[\gamma^y_{x,\text{int}} / \gamma^y_x, \gamma^y_{z,\text{int}} / \gamma^y_z\right]$	$> \delta_\xi\left(\gamma_{eq,DS3}\right)$
DS4	Failure/ Collapse	$> \gamma_u \cdot \min\left[\gamma^y_{x,\text{int}} / \gamma^y_x, \gamma^y_{z,\text{int}} / \gamma^y_z\right]$	$> \delta_\xi\left(\gamma_{eq,DS4}\right)$

Table 2: Damage state definitions for bridges with bearings and non-yielding piers of the wall type

2.3.3 Bridges with bearings and yielding piers of the column type

In this bridge typology the seismic energy is dissipated due to the inelastic behaviour of both piers and bearings. Thus, the shape of a 'typical' bridge pushover curve (Fig. 6) is similar to the previous bridge types. Here, the second branch represents both the successive plastic hinge formation and yielding of bearings. In addition, the slope of the first branch is smaller than in the case of bridges with yielding piers of the column type due to the significantly lower stiffness of pier-bearings systems, thus ultimate displacement ductility in

bridges with yielding piers of the column type is usually small, but is also a rather inappropriate indicator of the bridge's response. Damage states are defined using the corresponding definitions of bridges with yielding piers of the column type (Table 5, typically the μ_u<3.0 case applies).

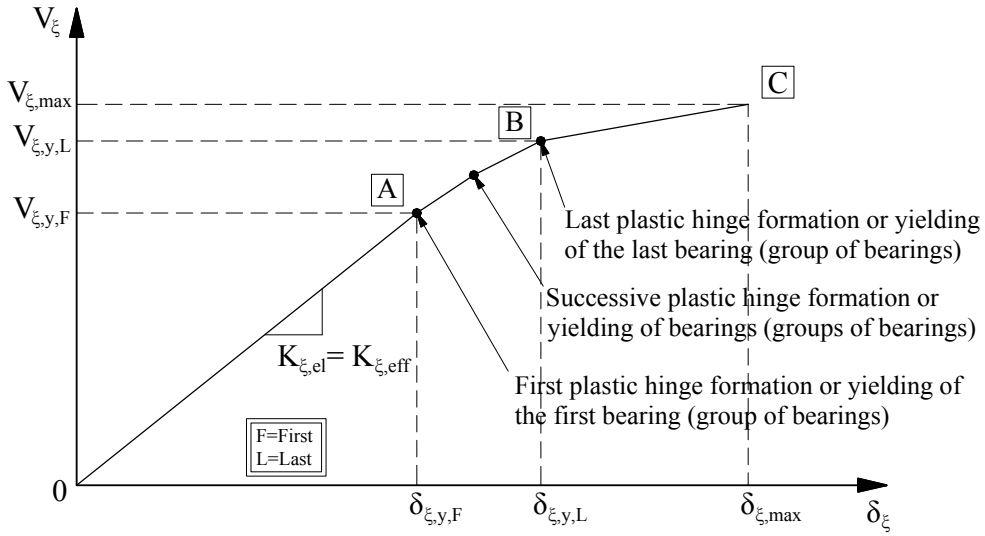

Figure 6: 'Typical' pushover curve of bridges with bearings and yielding piers of the column type.

a/a	Damage State	Threshold values of δ
DS1	Minor/Slight	$> 0.7 \cdot \delta_{\xi,y}$
DS2	Moderate	$> \delta_{\xi,y} + (1/3) \cdot (\delta_{\xi,u} - \delta_{\xi,y})$
DS3	Major/Extensive	$> \delta_{\xi,y} + (2/3) \cdot (\delta_{\xi,u} - \delta_{\xi,y})$
DS4	Failure/Collapse	$> \delta_{\xi,u}$

Table 3: Damage state definitions for bridges with bearings and yielding piers of the column type.

2.3.4 Damage due to abutment-backfill system activation

In case the abutment-backfill system is taken into account in the analysis model ('full-range analysis') the typical bridge pushover curve in the longitudinal direction has the shape shown in Fig. 7 (a bilinear force-displacement, *V*-δ, diagram is assumed for the abutment-backfill system). For deck displacements smaller than the longitudinal gap, δ_{gap}, the pushover curve is derived on the basis of bridge response. After the activation of the abutment-backfill system, its response is combined with bridge response and the pushover curve is derived adding the corresponding shear forces of bridge and abutment-backfill system for each value of bridge displacement.

Damage states are defined differently in the case where the abutment-backfill system is modelled (full-range analysis) and in the case where the abutment-backfill system is not directly included in the model (approximate analysis). In the former case (full range analysis) the first damage state is defined on the basis of the displacement at the longitudinal gap closure, δ_{gap}, the last damage state is defined on the basis of the ultimate displacement of the abutment-backfill system, if it is smaller than the ultimate bridge displacement δ_{max}, and the two intermediate damage states are defined at displacements equally spaced along the post-yield branch of the 'typical' bridge pushover curve after the activation of the abutment-backfill system. In the latter case (approximate analysis) the first damage state initiates at the gap closure, δ_{gap}. The two intermediate damage states are defined increasing the threshold

value of the first damage state by 10% and 20%, while the last damage state is defined as the maximum of $a \cdot \delta_u$ (which is an estimate for the ultimate displacement of the abutment-backfill system, see [8]) and $1.1 \cdot \delta_{DS3}$. When bridge ultimate displacement is smaller than these two values, δ_u is used to define the threshold of the final damage state.

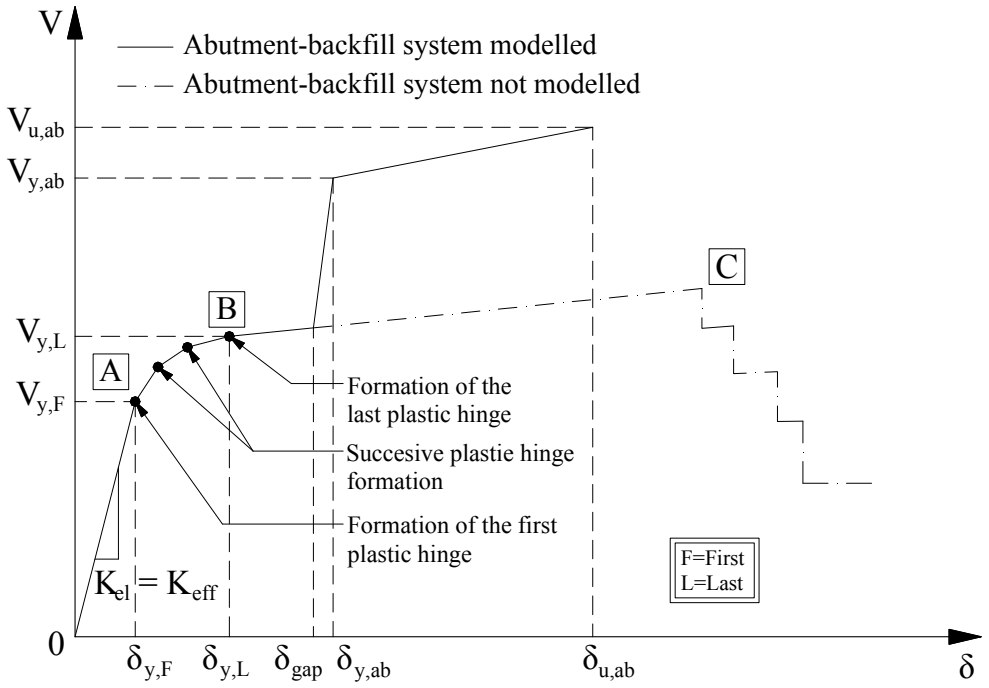

Figure 7: 'Typical' pushover bridge curve (here bridge with yielding piers of the column type) taking into account the abutment-backfill system.

a/a	Damage State	Threshold values of *Full range analysis*	*Approximate analysis*
DS1	Minor/Slight	$> \delta_{gap}$	$> \delta_{gap}$
DS2	Moderate	$> \delta_{y,ab} + (1/3) \cdot (\delta_{u,ab} - \delta_{y,ab})$	$> 1.1 \cdot \delta_{gap}$
DS3	Major/Extensive	$> \delta_{y,ab} + (2/3) \cdot (\delta_{u,ab} - \delta_{y,ab})$	$> 1.2 \cdot \delta_{gap}$
DS4	Failure/Collapse	$> \delta_{u,ab}$	$> \begin{cases} \delta_u, \text{ when } \delta_u < 1.1 \cdot \delta_{\Sigma B3} \\ \max\{a \cdot \delta_u, 1.1 \cdot \delta_{\Sigma B3}\} \end{cases}$

Table 4: Damage state definitions for damage developing at the abutment-backfill system.

The effect of the angle of incidence of the seismic action is taken into account by modifying bridge deck displacements estimated from static nonlinear analysis. More specifically, bridge displacement δ_ξ in the earthquake direction a, is firstly projected on the longitudinal bridge direction ($\delta_\xi \cdot \cos\alpha$ –Fig. 8a) and then it is increased by the displacement caused by the rotation of the bridge deck ($B \cdot \sin\theta$ – Fig. 8b). Hence, the bridge displacement $\delta_{\xi,Br}$, used in order to take into account the damage caused by the activation of the abutment-backfill system is

$$\delta_{\xi,Br} = \delta_\xi \cdot \cos a + B \cdot \sin a \tag{6}$$

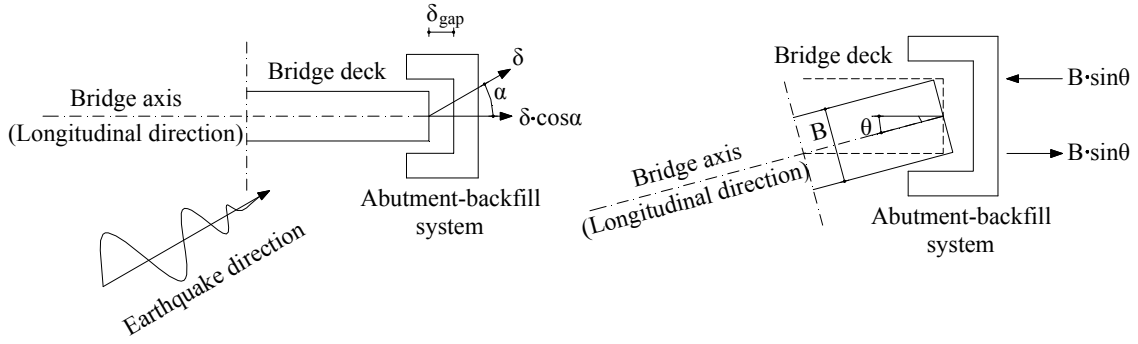

a. Projection of bridge displacement on the bridge axis

b. Increase of bridge displacement due to deck rotation

Figure 8: Calculation of bridge displacement for the activation of the abutment backfill system.

2.4 Derivation of fragility curves

The starting point for the derivation of fragility curves is the quantification of the exceedance of a given damage state, which is materialized using damage parameters, here bridge displacement δ_ξ along the axis $O\xi$ (Fig. 2) of the major horizontal component of the earthquake. Peak ground acceleration A_g is selected as the earthquake intensity parameter, but other quantities could also have been used (e.g. spectral displacement S_d).

The available bridge capacity that corresponds to the threshold of damage state i (i=1,2,3,4) is quantified through the bridge displacement δ_ξ used for the damage state definitions (Tables 1 to 4). Correspondingly, bridge response for a given earthquake intensity level A_g is quantified through bridge displacement $\delta_{\xi,Br|Ag}$, as it is calculated from bridge analysis for earthquake intensity A_g. Thus, the exceedance of a damage state can be represented by the following relationship

$$\delta_{\xi,Br|Ag} \geq \delta_{DSi} \tag{7}$$

and the probability of exceedance is written

$$P\left(\delta_{\xi,Br|Ag} \geq \delta_{DSi}\right) = P_f \tag{8}$$

In order to derive a fragility curve quantification of the total uncertainty is also needed. Here, since the probability density function is idealised as lognormal (as in most previous studies on bridge fragility), the total uncertainty is represented by the total lognormal standard deviation β_{tot}, which is assumed equal to 0.6 in line with previous studies [3]. The probability of exceedance using the median values of damage parameter (bridge displacement in the earthquake direction δ_ξ) can be written as:

$$P_f = \Phi\left[\frac{1}{\beta_{tot}} \cdot \ln\left(\frac{\delta_{\xi,Br,m|Ag}}{\delta_{DSi,m}}\right)\right] \tag{9}$$

The next step is the correlation of damage parameter (δ_ξ) with earthquake intensity parameter (A_g), which is achieved through the median damage evolution curve (or primary fragility curve, Fig. 10), which is the plot of the median value of bridge deck displacement versus the corresponding earthquake intensity parameter (here A_g). Fig. 9 shows the estimation of bridge displacement for increasing earthquake intensity levels using inelastic demand spectra in the region where the equal energy approximation is valid (i.e. for T≤0.5-0.6

sec) and elastic demand spectra in the region where the equal displacement approximation is valid (i.e. for T>0.5-0.6 sec). From the median damage evolution curve, given the threshold value of bridge deck displacement for a specific damage state, the corresponding median value of A_g can be estimated (Fig. 10). For example, the median threshold value of A_g for damage state DS2 for bridges with bearings and elastic piers of the wall type is the direction of the piers is that corresponding to $\delta_{DS2} = \delta(\gamma_{eq} = 1.5)$.

Hence, the damage state probability can be written in terms of peak ground acceleration A_g as follows:

$$P_f = \Phi\left[\frac{1}{\beta_{tot}} \cdot \ln\left(\frac{A_{g,m}}{A_{g,DSi,m}}\right)\right] \tag{10}$$

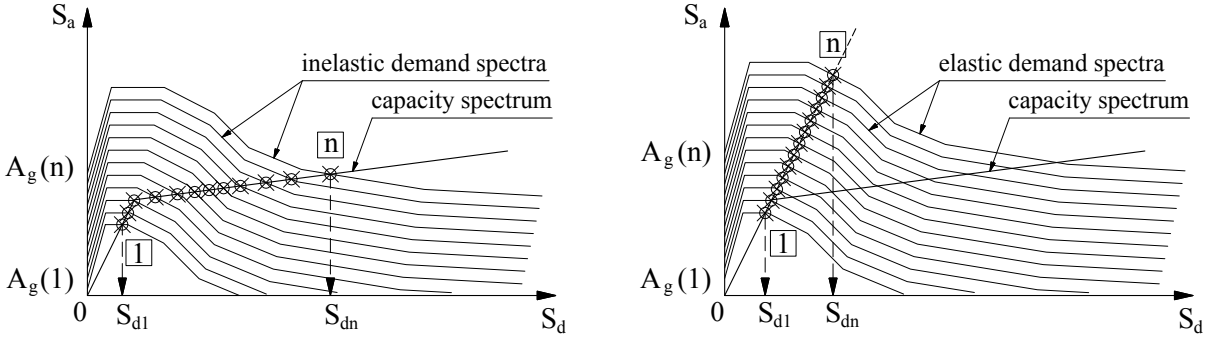

a. $T \leq$ 0.5-0.6 sec b. $T >$ 0.5-0.6 sec

Figure 9: Estimation of target displacement for increasing earthquake intensity levels

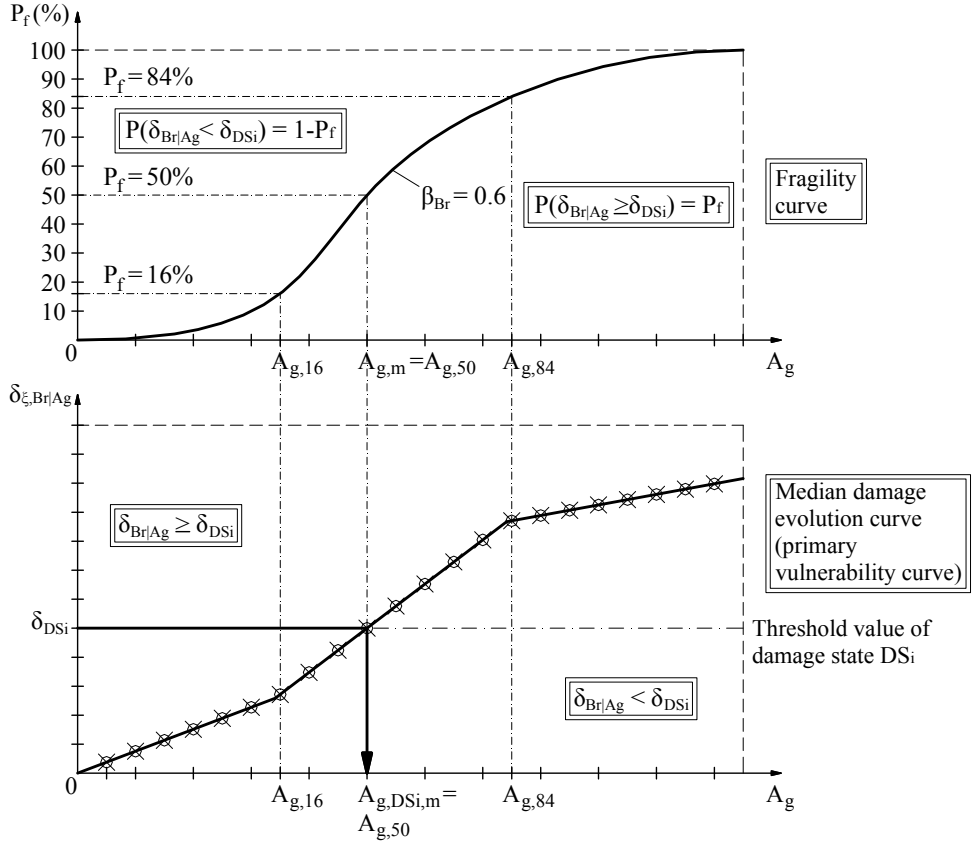

Figure 10: Median damage evolution curve (primary vulnerability curve) and fragility curve.

The plot of equation (10) is the fragility (probabilistic vulnerability) curve, of the specific damage state (Fig. 10). For the derivation of generalized fragility curves the proposed methodology is applied for various values of the angle of incidence of the seismic action between 0° and 180°.

3 APPLICATION OF THE PROPOSED METHODOLOGY TO SKEW BRIDGES

In a previous study by the authors [7] the proposed methodology was applied to a straight overpass bridge subjected to single-component seismic action. Here, the methodology is applied to a skew bridge subjected to either single- or dual-component seismic action.

3.1 Description and modelling of the selected bridge

The selected bridge is a 5-span bridge of 180m total length (5×36) that crosses Kosynthos River in North-Eastern Greece (Thrace), and is part of the Egnatia Motorway. The deck consists of a system with 6 simply-supported precast-prestressed beams connected through a continuous R/C slab (Fig. 11) and rests through common elastomeric bearings 400×500×181 (elastomer thickness 77mm) on four piers of the wall type with rectangular solid cross section 1.2×14.7m (Fig.12). Piers are inclined at an angle of 110° with respect to the bridge's longitudinal axis, i.e. there is a skew of 20^o (Fig. 13).

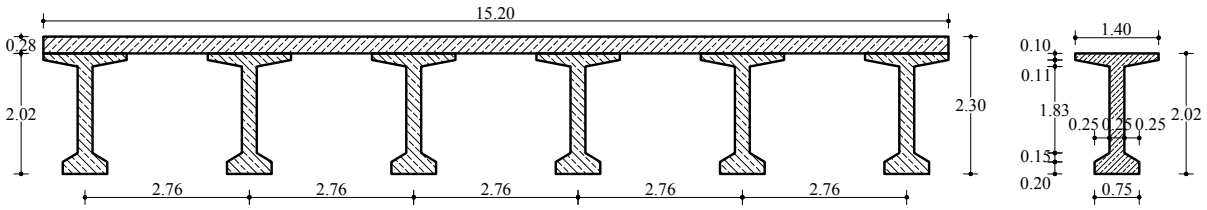

Figure 11: Deck section of Kosynthos bridge

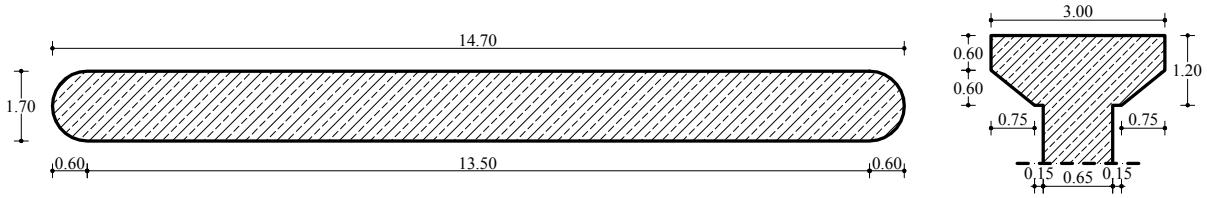

Figure 12: Wall-type pier section of Kosynthos bridge

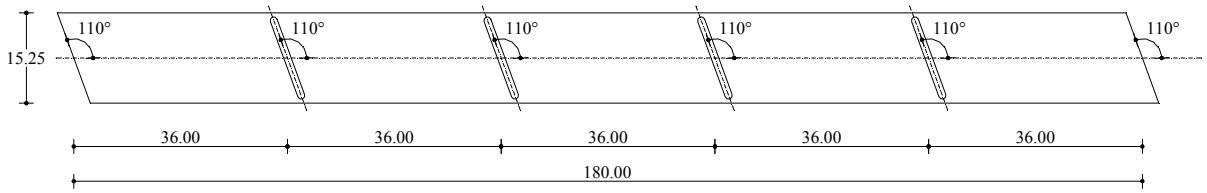

Figure 13: Inclination of pier in Kosynthos bridge with respect to the geometric longitudinal axis (Plan View)

The bridge deck rests on the abutments through common elastomeric bearings 400×600×226(110). The deck movement along the longitudinal direction is permitted up to the closure of a 100mm gap, while in the transverse direction it is unrestrained.

The Kosynthos bridge was modelled using the software package SAP2000 Nonlinear [2] (Fig.14a). Precast deck beams and piers are modelled with frame elements, while the

continuous deck slab is modelled with shell elements. Bridge bearings are modelled with Link elements with length equal to the total thickness of rubber in each bearing. The base of Link elements is connected through rigid-arms to the top of piers (Fig. 14b). The behaviour of bearings is considered as linear, which is a reasonable and common assumption for low-damping bearings (here the equivalent viscous damping is only about 5%).

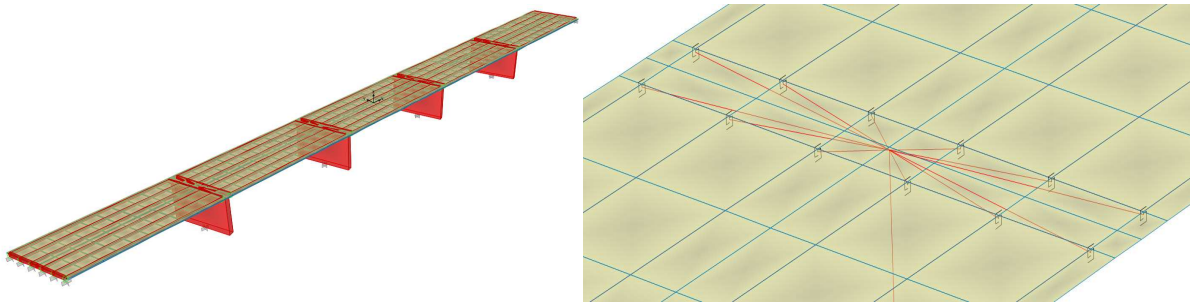

a. Finite element model

b. Modelling of pier-to-deck connection (through elastomeric bearings)

Figure 14: Modelling of Kosynthos bridge.

3.2 Application of the proposed methodology

The proposed methodology is applied twice, considering the seismic action either as single- component or as dual-component, for three different greek earthquakes using the records described in Table 5. For each of the three pairs, principal horizontal components are derived. The corresponding response spectra are shown in Fig. 15 for the case of Thessaloniki earthquake; it is worth pointing out that due to its different frequency content the minor component has larger spectral displacement values than the major one.

Place	Station	Date	Time	M	R [km]	Orientation	A_g [g]
Thessaloniki	City Hotel	20/6/78	08:03:21	6.1	29	N-S E-W	0.139 0.146
Kalamata	OTE Building	13/9/86	17:24:31	5.8	10	N80E N10W	0.240 0.272
Athens	Sepolia (Garage)	7/9/99	11:56:50	5.8	21	LONG TRANS	0.326 0.310

Table 5: Selected greek earthquakes.

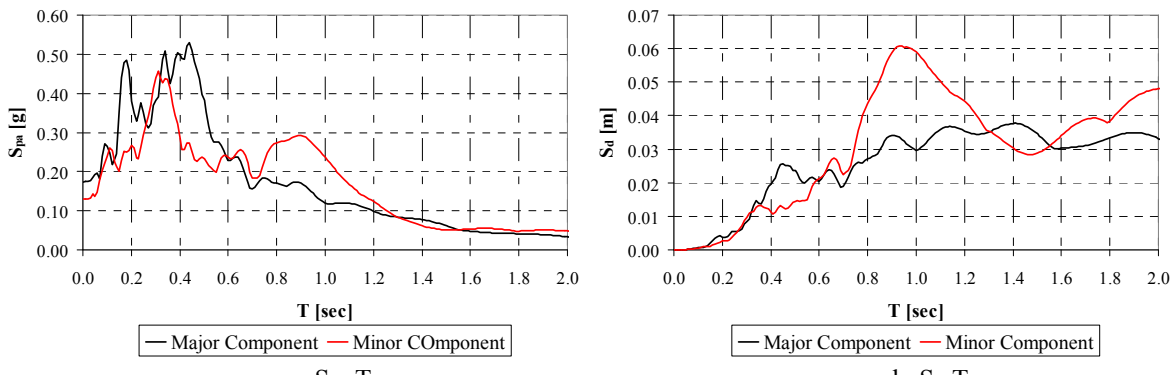

a. S_{pa}-T

b. S_d-T

Figure 15: Elastic response spectra of principal horizontal components of Thessaloniki earthquake.

For the derivation of pushover curves for arbitrary angle of incidence of the seismic action, the modal characteristics of the bridge have to be determined. The prevailing mode in the longitudinal direction is translational and the bridge deck moves as a rigid body at an angle of 20° with respect to the longitudinal axis (Fig. 16). The transverse prevailing mode is also translational but the deck moves as a rigid body at an angle of 110° with respect to the longitudinal axis (Fig. 17) or at an angle of 20° with respect to the geometric transverse axis, i.e. normal to the longitudinal prevailing mode. The two prevailing modes define the modal principal axes of Kosynthos bridge (Fig. 18, system O-*M*1-*M*2), which are rotated at an angle of 20° with respect to the geometric principal axes (Fig. 18, system *Oxy*). The rotation of the modal principal axes with respect to the geometric principal axes is due to the bridge skewness.

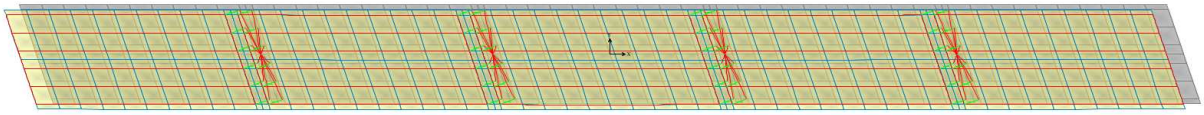

Figure 16: Prevailing longitudinal mode of Kosynthos bridge

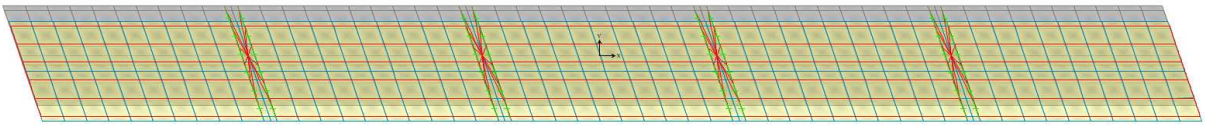

Figure 17: Prevailing transverse mode of Kosynthos bridge

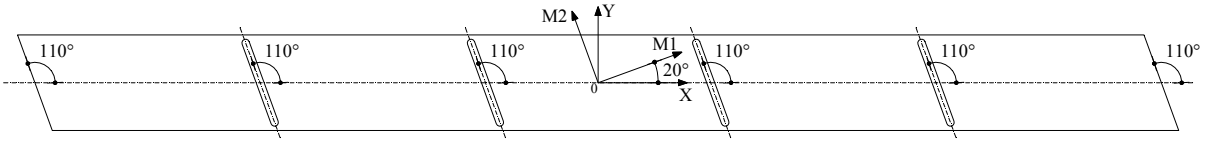

Figure 18: Geometric and modal principal axes of Kosynthos bridge

Regarding the periods of the two prevailing modes it is noticed (Table 6) that they differ only by 6.4%, something that is usual for bearing-supported bridges [8]. In addition, modal participating mass ratios are 100% for both prevailing modes along the corresponding modal principal axes, while with respect to the geometric principal axes they are $\varepsilon_x = \varepsilon_{M1} \cdot cos^2 20° = 88.3\%$ and $\varepsilon_y = \varepsilon_{M1} \cdot sin^2 20° = 11.7\%$ for the longitudinal prevailing mode and $\varepsilon_x = \varepsilon_{M2} \cdot sin^2 20° = 11.7\%$ and $\varepsilon_y = \varepsilon_{M2} \cdot sin^2 110° = 88.3\%$ for the prevailing transverse mode.

Prevailing mode	T [sec]	ε_x [%]	ε_y [%]	ε_{M1} [%]	ε_{M2} [%]
Longitudinal	1.376	88.3	11.7	100	0
Transverse	1.288	11.7	88.3	0	100

Table 6: Modal characteristics of the two prevailing modes of Kosynthos bridge

For force distribution consistent with the longitudinal and the transverse prevailing mode the bridge deforms only along the direction of modal principal axis *O*-*M*1 and *O*-*M*2, respectively. Thus, in order to apply the proposed methodology the modal principal directions are used instead of the corresponding geometric ones. Biaxial effects in the bridge bearings are ignored to simplify the procedure, keeping the modal principal axes constant; it is also noted that no information on shear and axial force interaction in bearings is available in the literature. The derived pushover curves, using the deck mass centre as control point, along the

modal principal directions are linear because the behaviour of common elastomeric bearing is considered as linear.

Then, the proposed methodology is applied for excitation angles from 0° to 110°, and the results are evaluated against those from linear dynamic analyses. In the single-component case the CQC rule is used for the combination of the projections of displacements of the control point and of base shears, because the earthquake components acting along the modal principal directions have identical accelerograms, hence identical response spectra, and the correlation of modal responses is significant (the modal correlation coefficient [16] is ρ_M = 0.696). Conversely, for the dual-component case the SRSS rule is adopted, ignoring the correlation of the earthquake components acting along the modal principal directions and the correlation of modal responses.

The key results from the application of the proposed methodology, i.e. displacement δ_ξ of the control point (deck mass centre) along the earthquake direction and the shear deformation of the equivalent single bearing γ_{eq} along the geometric principal directions, against the corresponding ones from the dynamics analyses, are shown in Tables 7 and 8 for single- and dual-component seismic action, respectively.

Focussing first on the results for the simpler case of the single-component seismic action, it is seen from Table 7 that the differences for δ_ξ are small for all excitation angles and vary from 0.0% for a=110° to 7.3% for a=60°. With respect to γ_{eq}, differences are similar to those for δ_ξ, varying from 0.0% for a=110° to 5.5% for a=60°.

When the minor principal horizontal component of the earthquake is also taken into account, differences are larger than in the single-component case, still small enough to be acceptable, varying from 0.1% for a=110° to 15.5% for a=45° for the displacement of the control point, and from 0.2% for a=110° to 13.1% for a=30° for the deformation of the equivalent shear bearing. Furthermore, differences are maximized for excitation angles a=30°, 45° and 60°, i.e. the region where correlation between the earthquake components acting along the modal principal bridge directions is maximized, something anticipated due to the use of the SRSS rule where the aforementioned correlation is ignored.

α [°]	δ_ξ [m]		Difference	$\gamma_{eq}=\max[\gamma_{eq,x}, \gamma_{eq,y}]$		Difference
	Static	Dynamic	[%]	Static	Dynamic	[%]
0	0.01598	0.01648	3.0	0.1517	0.1568	3.3
15	0.01645	0.01654	0.5	0.1494	0.1511	1.1
20 (M1)	0.01649	0.01656	0.4	0.1464	0.1467	0.2
30	0.01636	0.01656	1.2	0.1378	0.1354	1.7
45	0.01579	0.01655	4.6	0.1177	0.1132	3.8
60	0.01533	0.01654	7.3	0.1302	0.1378	5.5
75	0.01551	0.01659	6.5	0.1491	0.1553	4.0
90	0.01619	0.01667	2.9	0.1585	0.1623	2.4
105	0.01672	0.01676	0.3	0.1577	0.1587	0.6
110 (M2)	0.01677	0.01676	0.0	0.1549	0.1549	0.0

Table 7: Comparison between static and dynamic analysis results – Single-component seismic action.

The derived pushover curves for various excitation angles between 0° and 110° with a step of 15° (including the directions of modal principal directions) are also linear since the behaviour of common elastomeric bearings is considered as linear for both the single- and dual-component case. The most critical and least critical directions regarding bridge failure (bridge ultimate point) are for a=90° ($A_{g,u,min}$=2.80g) and a=45° ($A_{g,u,max}$=3.80g) for single-component seismic action, and for a=30 ($A_{g,u,min}$=1.80g) and a=75° ($A_{g,u,max}$=2.02g), i.e. for

the excitation angles where the maximum and the minimum value of the shear deformation of the equivalent single bearing is reached, for the dual-component action (Tables 7 and 8).

α [°]	δ_ξ [m]		Difference	$\gamma_{eq}=\max[\gamma_{eq,x}, \gamma_{eq,y}]$		Difference
	Static	Dynamic	[%]	Static	Dynamic	[%]
0	0.01696	0.01790	5.2	0.2297	0.2306	0.4
15	0.01601	0.01692	5.4	0.2319	0.2225	4.1
20 (M1)	0.01651	0.01655	0.3	0.2299	0.2168	5.7
30	0.01858	0.01651	11.1	0.2483	0.2158	13.1
45	0.02101	0.01775	15.5	0.2433	0.2342	3.7
60	0.02129	0.01820	14.5	0.2285	0.2436	6.2
75	0.01927	0.01780	7.7	0.2220	0.2445	9.2
90	0.01698	0.01658	2.4	0.2318	0.2401	3.4
105	0.01629	0.01646	1.0	0.2321	0.2356	1.5
110 (M2)	0.01677	0.01678	0.1	0.2315	0.2318	0.2

Table 8: Comparison between static and dynamic analysis results – Dual-component seismic action.

Finally, generalized fragility curves for various excitation angles are derived (Figures 19 to 26) for both the single- and the dual-component case. The corresponding median damage state threshold values of peak ground acceleration are shown in Table 9. It is observed that in the case of single-component seismic action, for all damage states, the critical bridge direction is a=90°, while the less critical direction is a=45°. When the minor principal earthquake component is also taken into account the critical direction is a=30° while the least critical one is a=75°. It is also observed that for both in single- and dual-component seismic action the most critical and the least critical directions are similar with those resulting from the pushover curves, because the ultimate bridge point and the damage state definitions are based on the shear deformation of the equivalent single bearing.

α [°]	Singe-Component Seismic Action				Dual-Component Seismic Action			
	DS1	DS2	DS3	DS4	DS1	DS2	DS3	DS4
0	0.132	0.989	1.319	2.951	0.087	0.653	0.871	1.948
15	0.134	1.004	1.338	2.995	0.086	0.647	0.862	1.930
20 (M1)	0.137	1.025	1.366	3.058	0.087	0.653	0.870	1.947
30	0.145	1.089	1.452	3.249	0.081	0.604	0.806	1.803
45	0.170	1.274	1.699	3.803	0.082	0.616	0.822	1.840
60	0.154	1.152	1.536	3.437	0.088	0.656	0.875	1.959
75	0.134	1.006	1.342	3.003	0.090	0.676	0.901	2.016
90	0.126	0.947	1.262	2.824	0.086	0.647	0.863	1.931
105	0.127	0.951	1.268	2.839	0.086	0.646	0.862	1.929
110 (M2)	0.129	0.968	1.291	2.889	0.086	0.648	0.864	1.934

Table 9: Median values of damage state thresholds in terms of peak ground acceleration A_g for Kosynthos bridge, for all excitation angles

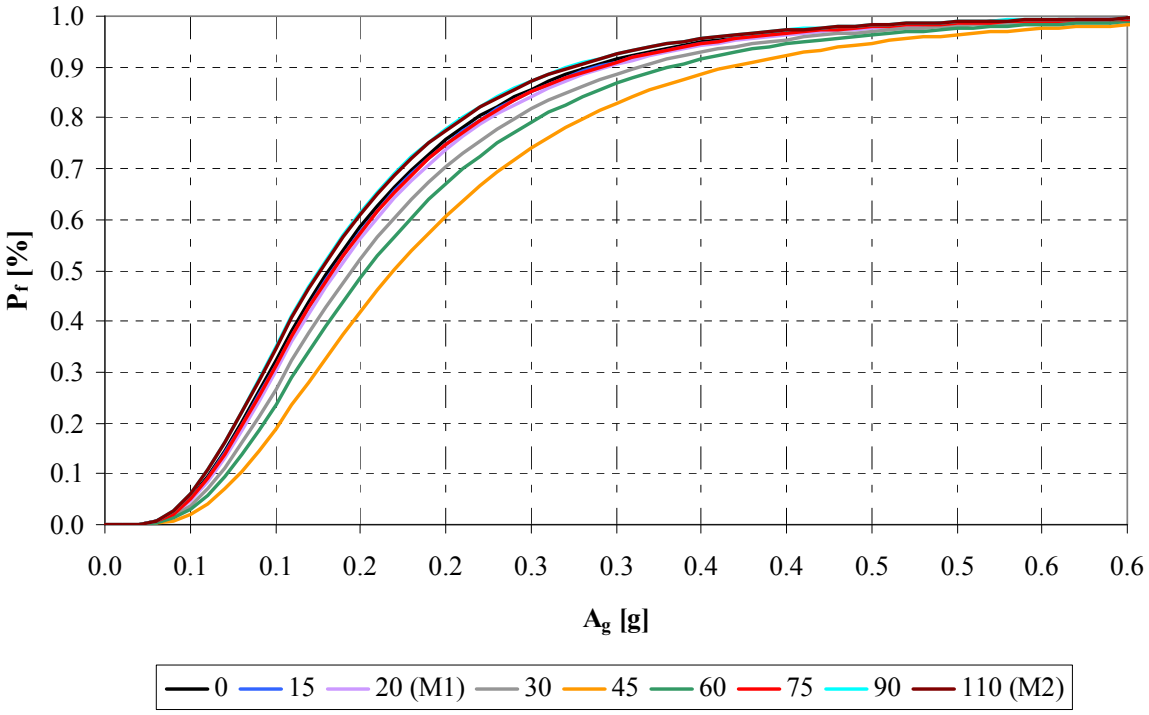

Figure 19: Generalized fragility curves of Kosynthos bridge for single-component seismic action, DS1: Minor/Slight Damage.

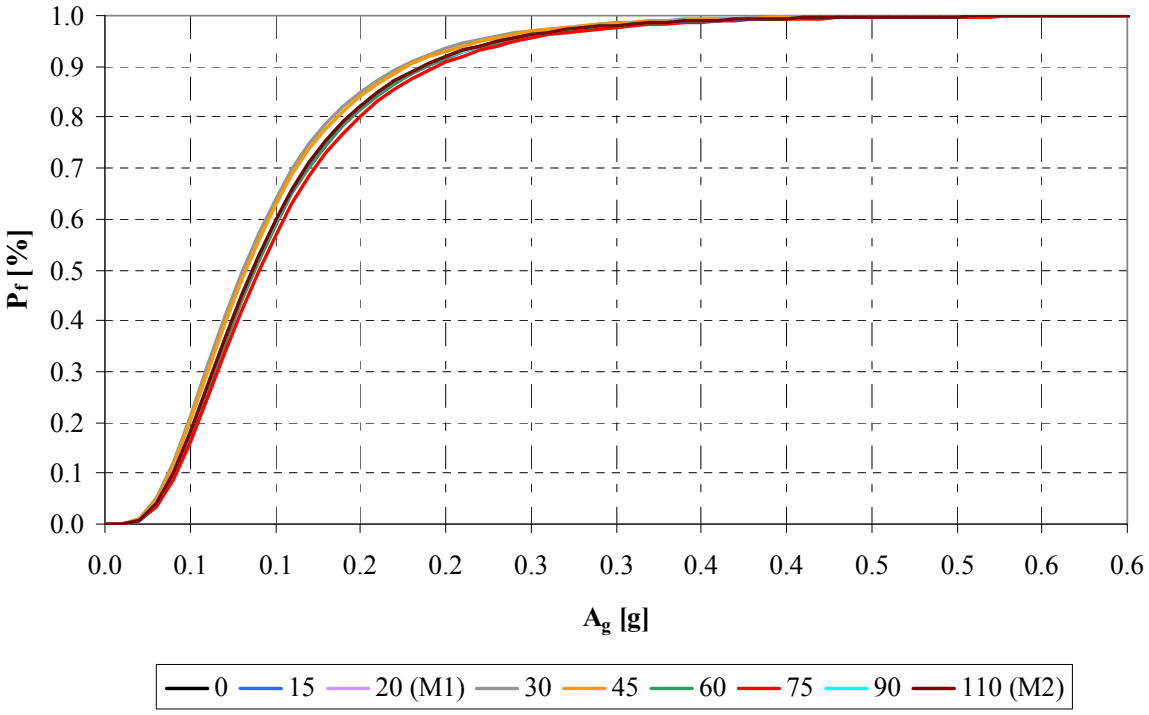

Figure 20: Generalized fragility curves of Kosynthos bridge for dual-component seismic action, DS1: Minor/Slight Damage.

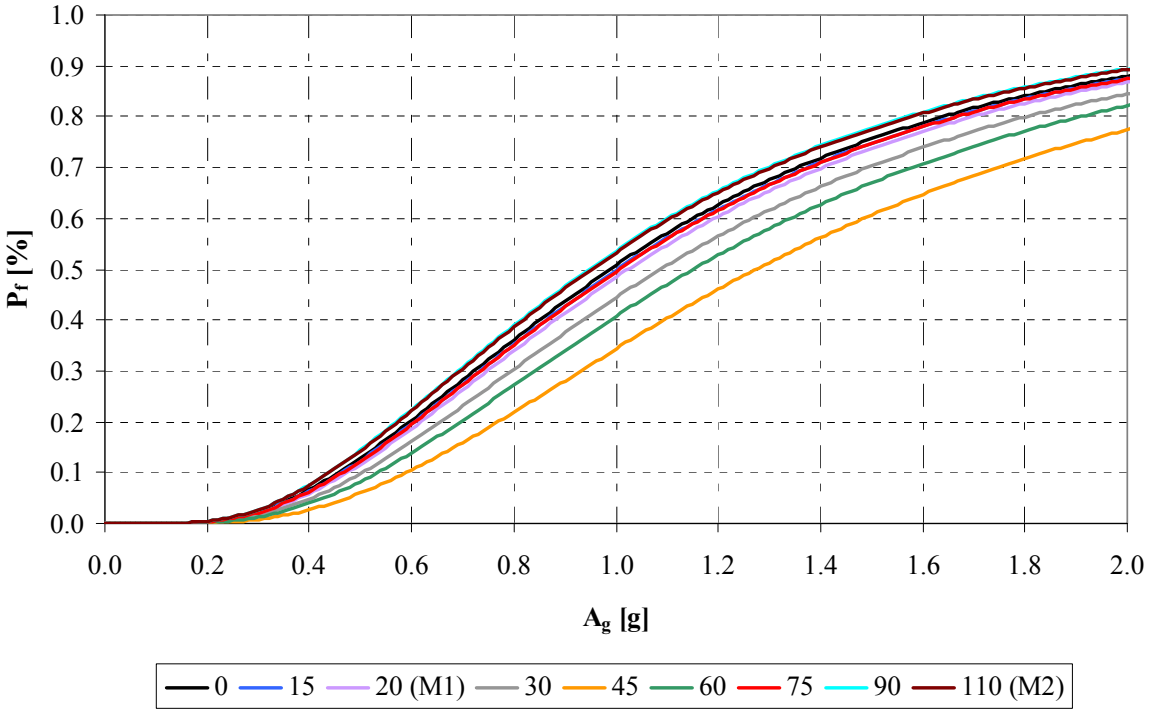

Figure 21: Generalized fragility curves of Kosynthos bridge for single-component seismic action, DS2: Moderate Damage.

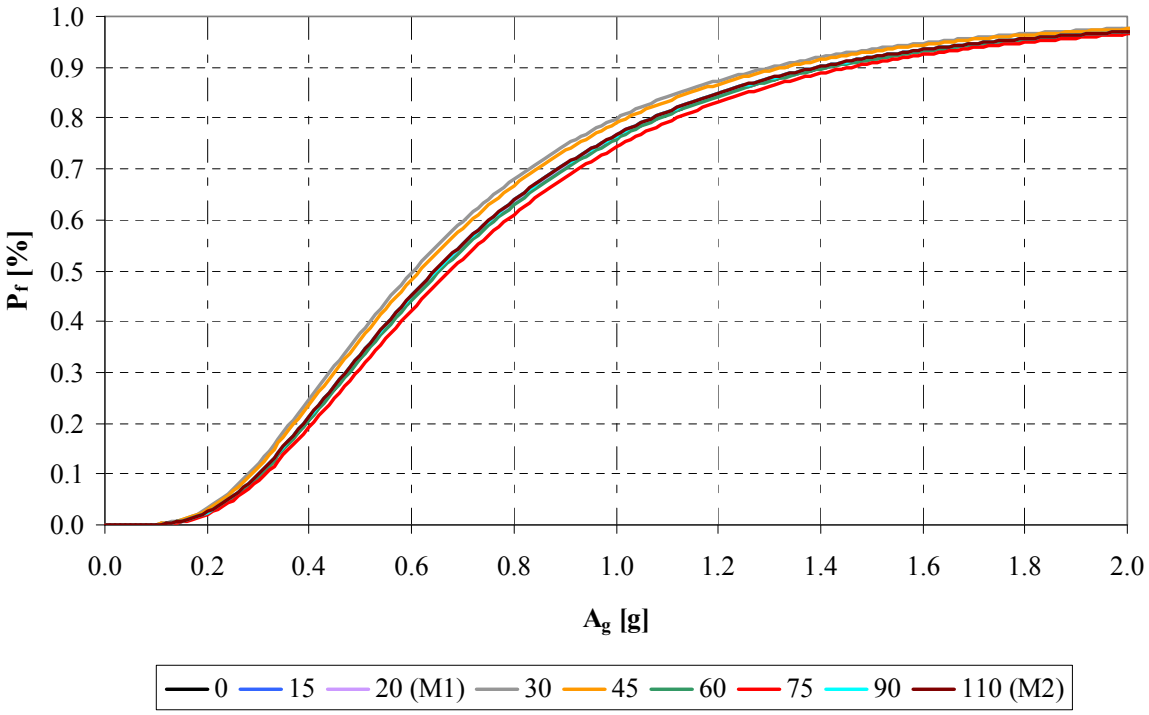

Figure 22: Generalized fragility curves of Kosynthos bridge for dual-component seismic action, DS2: Moderate Damage.

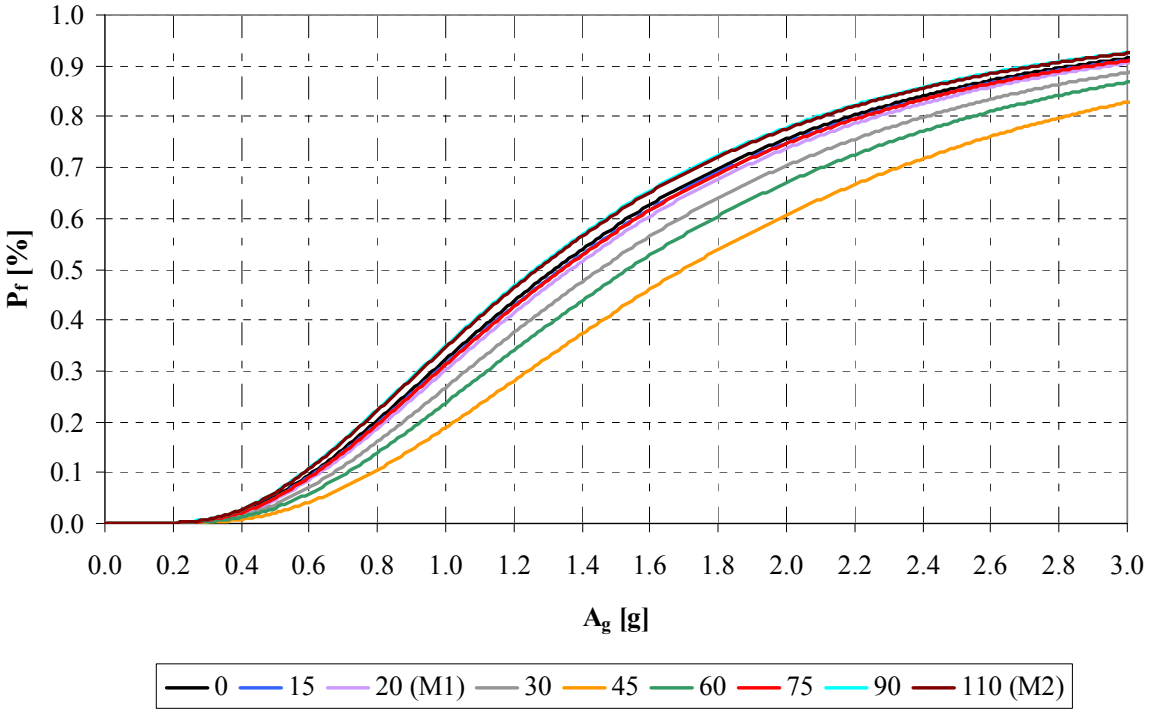

Figure 23: Generalized fragility curves of Kosynthos bridge for single-component seismic action, DS3: Major/Extensive Damage.

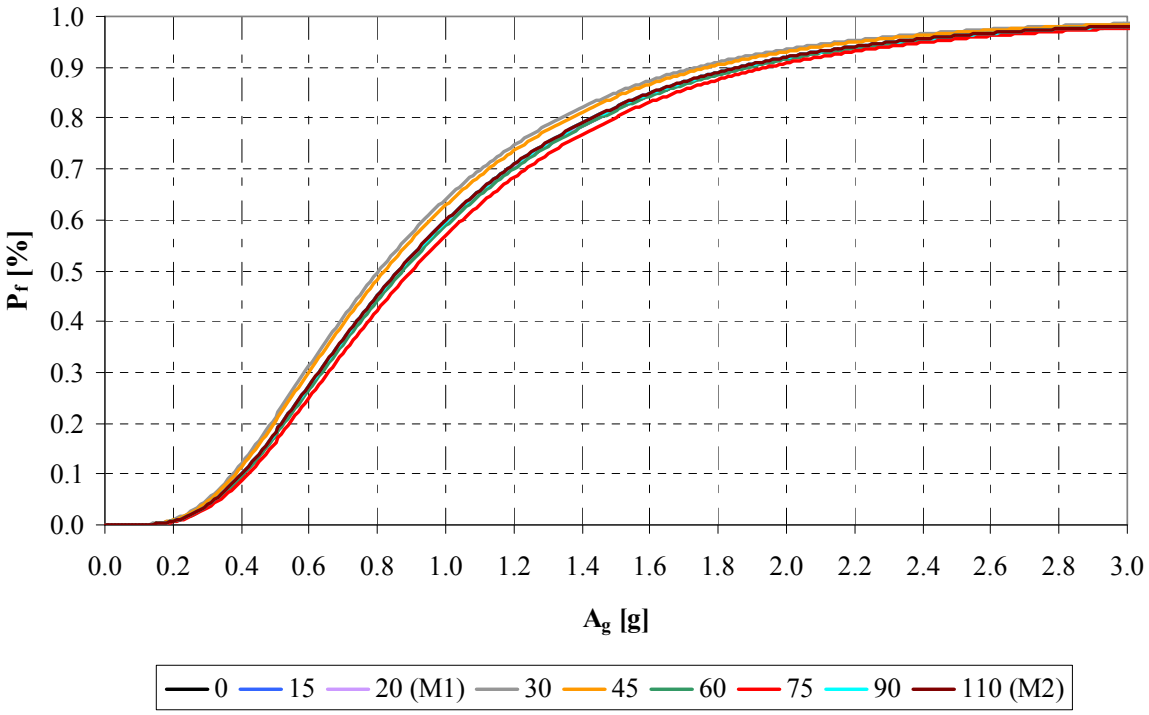

Figure 24: Generalized fragility curves of Kosynthos bridge for dual-component seismic action, DS3: Major/Extensive Damage.

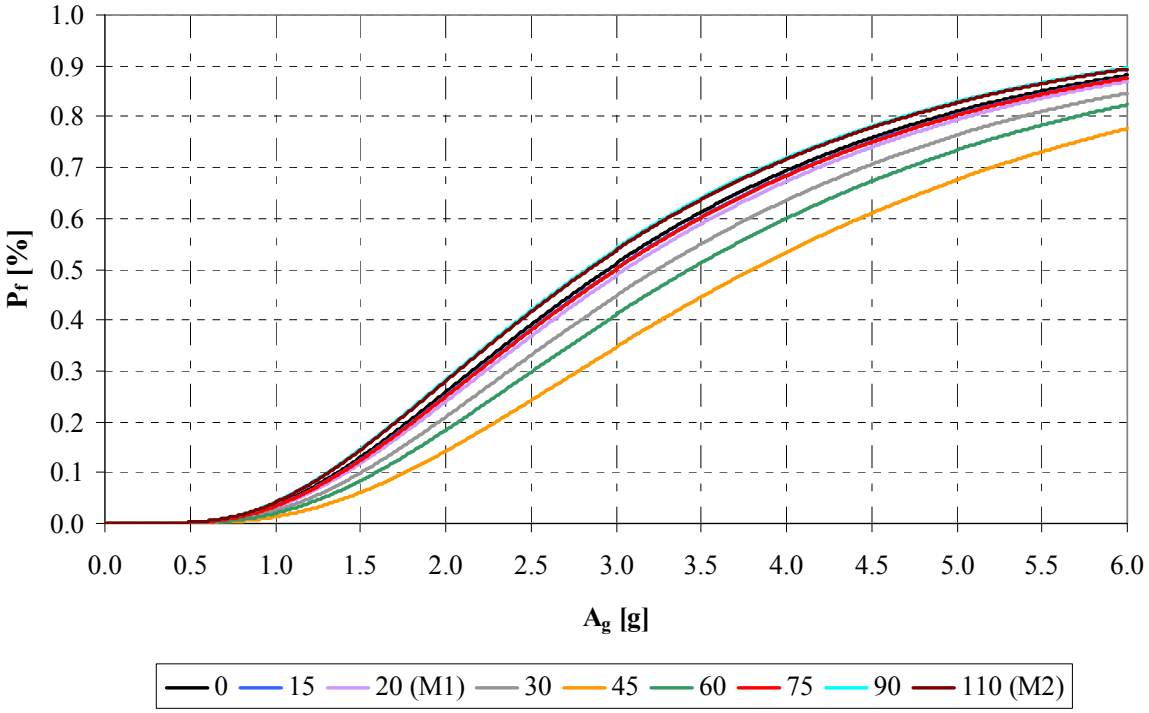

Figure 25: Generalized fragility curves of Kosynthos bridge for single-component seismic action, DS4: Failure/Collapse.

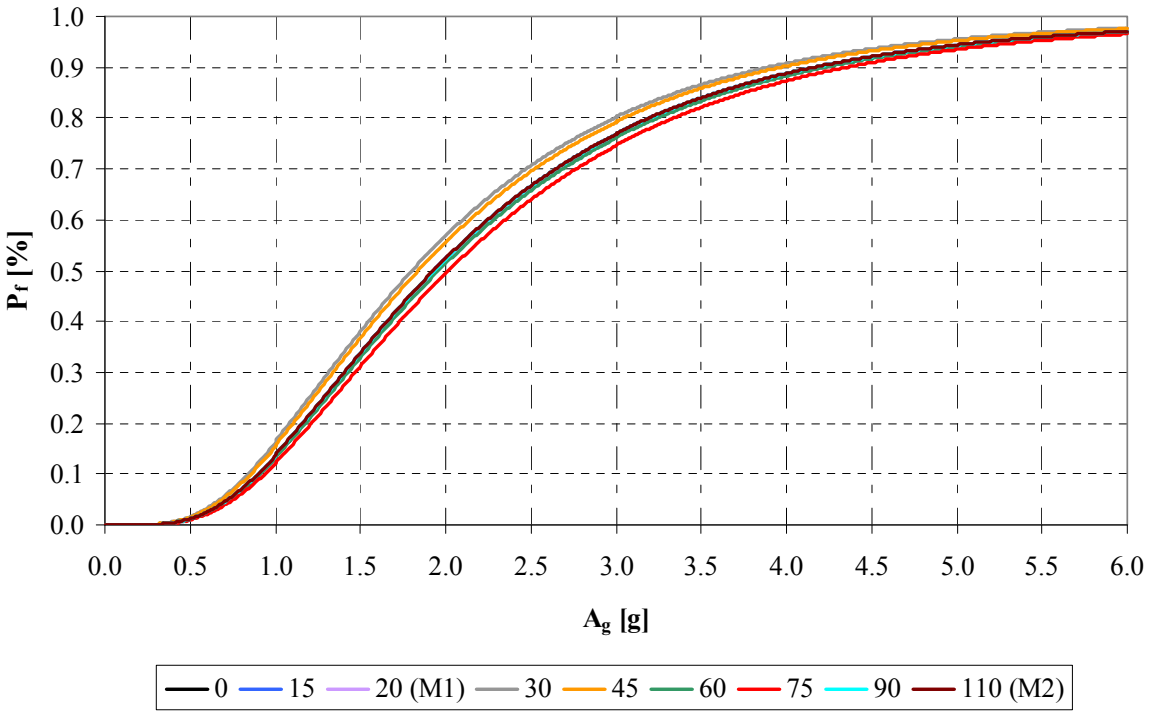

Figure 26: Generalized fragility curves of Kosynthos bridge for dual-component seismic action, DS4: Failure/Collapse.

It is important to point out that when the minor principal component is considered in the analysis, median threshold values of A_g are reduced by 41.6%, indicated a significant increase in bridge fragility, for all excitation angles. Finally, the maximum and the minimum median threshold values of A_g differ by 25.7% in the single-component case, while in the dual-component case the difference is reduced to 10.5%. This suggests that bridge fragility remains practically insensitive to the earthquake direction when the minor principal component of the earthquake is taken into account.

4 CONCLUDING REMARKS

A methodology for bridge fragility analysis under arbitrary angle of incidence of the earthquake, previously proposed by the authors [7], was extended here to take into account the minor principal horizontal component of the earthquake (dual-component seismic action). Furthermore, damage states for the case of bearing-supported bridges were redefined in a broader manner in order to take into account the interaction between biaxial shear and axial load, as well as all possible failure mechanisms, of the bearings. The proposed methodology was applied to an actual skew bridge for both single- and dual-component seismic action.

In skew bridges modal principal directions are not identical to geometric principal bridge directions, as in straight bridges, but they are rotated at a specific angle. According to the proposed methodology standard pushover analyses are performed for force distributions consistent with each of the prevailing bridge modes (longitudinal-transverse). Thus, modal principal bridge directions are used for the application of the proposed methodology. In the single-component case the CQC rule is used for the combination of the projections of the control point displacement and of the base shear, due to the significant correlation of modal responses in bearing-supported bridges. Conversely, in the dual-component case the SRSS rule is used, ignoring the correlation between the modal responses and also the earthquake components acting along the modal principal bridge directions. The expected differences in the range of excitation angles wherein the correlation between the earthquake components acting along modal principal direction is maximized are reasonably small (15%), showing the validity of the use of the SRSS rule in the dual-component case, for all excitation angles.

From the derived generalized fragility curves for arbitrary angle of incidence of seismic action it was seen that when the minor principal horizontal component is taken into account bridge fragility is significantly increased (more than 40% in the studied skew bridge), whereas it remains almost unaffected by the angle of incidence of the seismic action.

REFERENCES

[1] N.I. Basöz, A.S. Kiremidjian, *Evaluation of Bridge Damage Data from the Loma Prieta and Northridge, California Earthquakes*. *Technical Report MCEER-98-0004*, Multidisciplinary Center for Earthquake Engineering Research (MCEER), State University of New York at Buffalo, 1998.

[2] CSI, *CSI Analysis Reference Manual for SAP2000®, ETABS®, and SAFE®*, Computers & Structures Inc., Berkeley, California, USA, 2009.

[3] FEMA-NIBS, *Multi-Hazard Loss Estimation Methodology - HAZUS-MH MR4: Earthquake Model Technical Manual*, Federal Emergency Management Agency (under a contract with the National Institute of Building Sciences), Washington, D.C., 2003.

[4] K.R. Karim, F. Yamazaki, A simplified method of constructing fragility curves for highway bridges. *Earthquake Engineering & Structural Dynamics*, **32,** 1603-1626, 2003.

[5] O.A. López, J. J. Hernández, R. Bonilla, A. Fernández, Response spectra for multicomponent structural analysis. Earthquake Spectra, **22**, 85-113, 2006.

[6] K.R. Mackie, B. Stojadinović, R-factor parameterized bridge damage fragility curves. *Journal of Bridge Engineering*, *ASCE*, **12**, 500-510, 2007.

[7] I.F. Moschonas, A.J. Kappos, Generalized fragility curves for bridges, for arbitrary angle of incidence. *COMPDYN 2009*, CD-ROM Proceedings: Paper No. 186, Rhodes, Greece, June 22-24, 2009.

[8] I.F. Moschonas, A.J. Kappos, P. Panetsos, V. Papadopoulos, T. Makarios, P. Thanopoulos, Seismic fragility curves for greek bridges: methodology and case studies. *Bulletin of Earthquake Engineering*, **7**, 439-468, 2009.

[9] B.G. Nielson, R. DesRoches, Seismic fragility methodology for highway bridges using a component level approach. Earthquake *Engineering & Structural Dynamics*, **36**, 823-839, 2007.

[10] J.E. Padgett, R. DesRoches, Methodology for the development of analytical fragility curves for retrofitted bridges. *Earthquake Engineering & Structural Dynamics*, **37**, 1157-1174, 2008.

[11] G. Panagopoulos, A.J. Kappos, Bilinear idealization of force deformation diagrams. *16th Hellenic Conference on Concrete*, CD-ROM Proceedings: Paper No. 121105, Pafos, Cyprus, October 21-23, 2009 (*in Greek*).

[12] M. Shinozuka, S. Banerjee, S.H. Kim, *Statistical and Mechanistic Fragility Analysis of Concrete Bridges*. *Technical Report MCEER-07-0015*, Multidisciplinary Center for Earthquake Engineering Research (MCEER), State University of New York at Buffalo, 2007.

[13] M. Shinozuka, M.Q. Feng, H. Kim, S. Kim, Nonlinear Static Procedure for Fragility Curve Development. *Journal of Engineering Mechanics*, *ASCE*, **126**, 1287-1295, 2000.

[14] B. Song, J.S. Pan, Q. Liu, Study on critical angle to the seismic response of curved bridges based on pushover method. *14th World Conference on Earthquake Engineering*, CD-ROM Proceedings: Paper No. 14-0120, Beijing, China, October 12-17, 2008.

[15] B. Song, R. Yang, H. Shan, Determination of critical angle of seismic wave in safety evaluation of curved bridges. *International Symposium on Safety Science and Technology*, 2319-2324, Changsha, Hunan, China, October 12-17, 2006.

[16] E.L. Wilson, A. Der Kiureghian, E.P. Bayo. A replacement for the SRSS method in seismic analysis. *Earthquake Engineering & Structural Dynamics*, **9**, 187-192, 1981.